The Astrophysical Journal, 805:165 (12pp), 2015 June 1 doi:10.1088/0004-637X/805/2/165

EFFECTS OF SOLAR SURFACE MAGNETIC FIELDS ON THE TIME–DISTANCE ANALYSIS OF SOLAR SUBSURFACE MERIDIONAL FLOWS

Zhi-Chao Liang and Dean-Yi Chou
Physics Department, National Tsing Hua University, Hsinchu, 30013, Taiwan; chou@phys.nthu.edu.tw
Received 2015 January 4; accepted 2015 March 26; published 2015 May 29

ABSTRACT

The solar meridional flow in the deep convection zone can be measured with time–distance analysis. The difference between northward and southward acoustic wave travel times relates to the speed of meridional flow in the solar convection zone. We study the effects of surface magnetic field on the measured travel time difference in time–distance analysis by comparing the results using data with and without removing surface magnetic regions. Two results are significantly different if the field strength threshold used to remove magnetic regions is small enough, such as 50 G. The difference represents the surface magnetic effects. This difference strongly correlates with the sunspot number. The range of travel distance in this study is 7°–75°, corresponding to a depth range of $0.54-0.96\,R_{\odot}$. The difference depends on the travel time distance, and is greatest for the travel distance of 11°−20°. The study with different field strength thresholds indicates that a threshold of about 50 G can remove most surface magnetic effects. The measured surface magnetic effects can be explained by an effective downflow inside magnetic regions. These signals are not related to the large-scale meridional flow; they need to be considered in the measured travel time difference even when activity is low, if the travel time difference is used to infer meridional flow signals.

Key words: Sun: activity – Sun: evolution – Sun: helioseismology – Sun: interior – Sun: magnetic fields – Sun: oscillations

1. INTRODUCTION

The meridional flow is a large-scale axisymmetric circulating flow on meridional planes. It has poleward motion on the surface and penetrates into the solar interior. It was originally proposed to balance the latitudinal dependence of energy transport due to rotation (Durney & Roxburgh 1971). The meridional flow plays an important role in the dynamics of the Sun. It can also be used to probe the temporal variations of the solar interior.

The surface meridional flow can be measured with the tracers on the surface (Howard & Gilman 1986; Komm et al. 1993; Snodgrass & Dailey 1996; Meunier 1999; Svanda et al. 2007; Hathaway & Rightmire 2010) or directly with Doppler shifts on the surface (Duvall 1979; LaBonte & Howard 1982; Hathaway et al. 1996; Ulrich 2010). The speed of poleward motion on the surface versus latitude has an approximate sine-shape distribution, with a magnitude of 10–20 $\mathrm{m\,s^{-1}}$. The subsurface meridional flow can be measured with helioseismic methods, such as ring-diagram analysis (Basu et al. 1999; Basu & Antia 2000; Gonzalez Hernandez et al. 2008), frequency-shift measurements (Braun & Fan 1998), eigenfunction perturbation analysis (Schad et al. 2011, 2013), and the time–distance method (Giles et al. 1997; Giles 1999; Chou & Dai 2001; Beck et al. 2002; Zhao & Kosvichev 2004; Chou & Ladenkov 2005; Zhao et al. 2013; Kholikov & Hill 2014; Kholikov et al. 2014). For the meridional flow in the deep convection zone, the time–distance method is most commonly adopted.

The solar *p*-mode wave is trapped in a cavity between the surface and a subsurface layer. The acoustic signal propagates from the surface downward to the bottom of the cavity and back to the surface at a horizontal distance from the original point. Different *p*-modes have different paths; they penetrate into different depths and arrive at the surface with different travel distances and times. The *p*-modes with the same horizontal phase speed have approximately the same ray path. The relation between the travel time and distance for different *p*-modes was first measured by Duvall et al. (1993) using the temporal cross correlation between two surface points. The wave associated with a greater horizontal phase speed, corresponding to a longer horizontal wavelength, has a greater travel distance and penetrates deeper into the solar interior. Thus, waves with different travel distances can be used to probe different depths of the solar interior.

The travel time determined from the cross-correlation function (CCF) is the integral of travel time along the wave path between two surface points. It depends on the wave speed and flow speed along the wave path. The mean of travel times of opposite directions depends on the wave speed along the wave path, while the difference of opposite directions depends only on the flow speed to the lowest order (Duvall et al. 1996; Kosovichev 1996). Thus, the travel time difference measured with a pair of points at the same longitude carries information of meridional flow along the wave path between the two points. Using different pairs at different latitudes for different travel distances at different times allows us to study meridional flow as a function of latitude, depth, and time.

It is known that magnetic fields complicate Doppler measurements in magnetic regions. Besides the influence of magnetic fields on spectroscopic measurements, there may exist flows other than meridional flow inside magnetic regions. The influence of magnetic regions on the measurements of meridional flow in the upper convection zone has been investigated with ring-diagram analysis (Gonzalez Hernandez et al. 2008) and time–distance analysis (Gizon 2003). In this study, we investigate the effects of surface magnetic regions on the measurements of travel time difference in time–distance

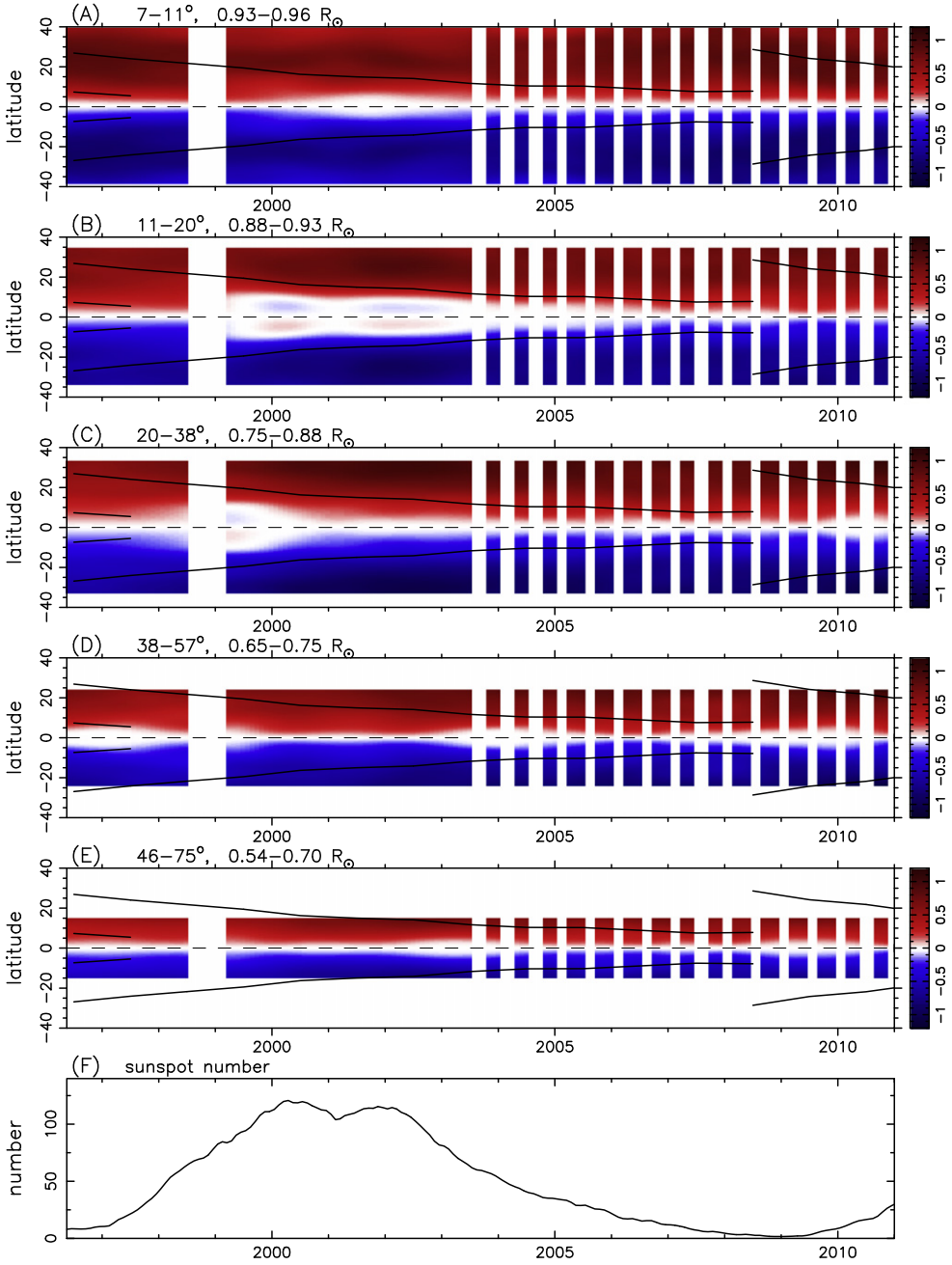

Figure 1. Panels (A)–(E): travel time difference $\delta\tau_\infty$, without surface magnetic effect removed, as a function of latitude and time for different travel distances. The range of travel distance and the corresponding radii of lower-turning layers from ray approximation are indicated at the top of each panel. The positive value (red) corresponds to northward motion and the negative (blue) to southward motion. Only the antisymmetric component is kept (see the text). The unit in the color bar is second. A Gaussian smoothing, with FWHM = 7°.2 in latitude and one year in time, is applied to show the large-scale variations. The black line marks the center of active latitudes in each hemisphere. The tick of year indicates the beginning of the year. The blank in 1998 and 1999 is caused by the spacecraft loss. Half of the data after July of 2003, when the MDI instruments flipped 180°, are not used here to ensure consistency. Panel (F): sunspot numbers vs. time.

analysis in detecting the subsurface meridional flow in the range of 0.54−0.96 $R_\odot$.

In Section 2, we describe the data and analysis. In Section 3, we compare the travel time differences with and without removing surface magnetic effects, and discuss the surface magnetic effects. In Section 4, we investigate the effects of the different thresholds used for removing magnetic regions. In Section 5, we investigate the surface magnetic effects on the mean travel time.

2. DATA AND ANALYSIS

In this study, we use 15 yr data taken with the Michelson Doppler Imager (MDI) on board the *Solar and Heliospheric Observatory* (*SOHO*) spacecraft (Scherrer et al. 1995). They are full-disk Doppler images of 192 × 192 pixels, sampled at a rate of one image per minute. Each time series of 24 hr is analyzed separately. The data analysis procedure is briefly described as follows. (1) A Hann-window temporal filter is

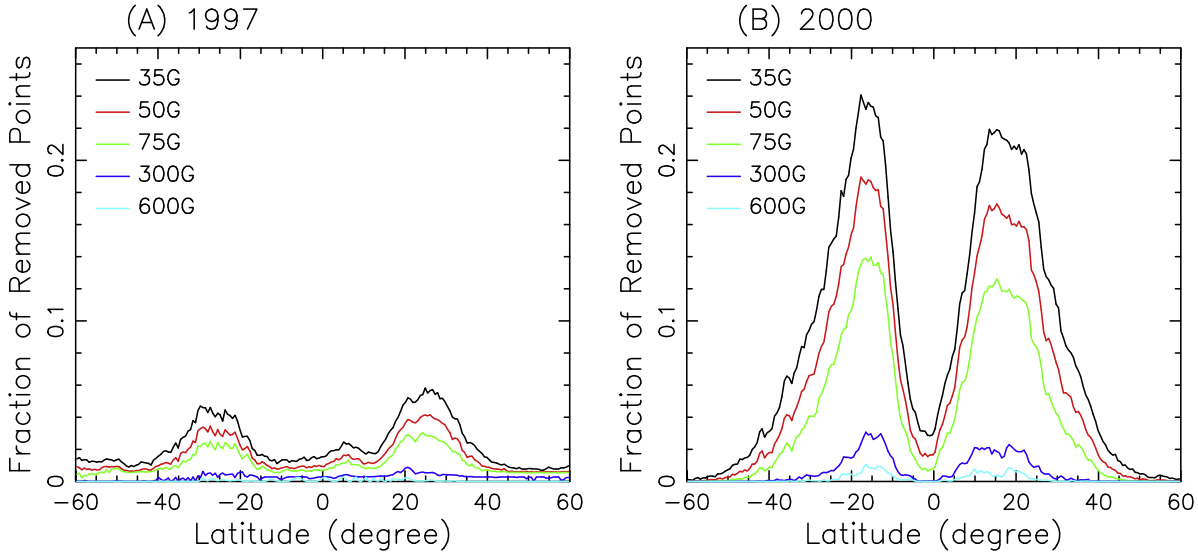

Figure 2. Fraction of data points removed at each latitude for different magnetic thresholds. Panel (A) is for year 1997, and panel (B) year 2000 (maximum).

applied to remove signals below 1.5 mHz. No other filter has been applied in this study to avoid the spreading of the influence of magnetic regions. (2) Each image is transformed into the longitude–latitude coordinates with a step size of 0.°6 in both directions. (3) The surface differential rotation is removed (Chou et al. 2009). (4) For each point, two arcs of 30° in the north–south direction with the same distance to the central point are selected. The CCF between a pair of opposite points on the two arcs is computed, and then the CCF's of the different pairs on the arcs are averaged. The result is assigned to the central point. (5) The computation of the arc-averaged CCF is repeated for different central points. Each step is 0.°6 in latitude. For each latitude, the CCF's are averaged over ±45° longitude to enhance the signal-to-noise ratio (S/N). (6) The northward and southward travel times are determined from the cross-correlation function. Here we use two different methods for determining the travel time. One is to fit the instantaneous phase of the CCF (Bracewell 1986; Chou & Serebryanskiy 2001). The other is the method developed by Gizon & Birch (2002). The difference between the two results is negligibly small in this study. In the following discussion, we present only the results from the former method. (7) The difference between opposite-direction travel times, denoted as $\delta\tau$, carries information of meridional flow along the wave path. The positive $\delta\tau$ corresponds to the northward motion and the negative the southward motion.

The above computation is repeated for different latitudes and travel distances for each data set of 24 hr to obtain $\delta\tau$ as a function of latitude and depth. This procedure is repeated for all data sets to obtain the solar-cycle variations of $\delta\tau$. Half of the data after 2003 July, when the MDI instruments flipped 180°, are not used here to ensure consistency.

The travel time difference $\delta\tau$ is proportional to a weighted average of the flow velocity along the entire wave path, but the significant contribution comes from the flow near lower-turning layer (Giles 1999), unless there are vertical flows near the surface. Thus, $\delta\tau$ reflects the meridional flow around the lower-turning layer associated with the travel distance. The larger the travel distance, the deeper the lower-turning layer.

The travel time difference $\delta\tau$ is averaged over a travel distance range to enhance S/N. The results of five travel distance ranges, as a function of latitude and time, are shown in Figure 1. The travel time difference is denoted as $\delta\tau_\infty$ to indicate no surface effect has been removed (removed with an infinity threshold). The range of travel distance in averaging and the range of the corresponding lower-turning layer are shown at the top of each panel. Only the antisymmetric component of $\delta\tau_\infty$ is kept to remove contamination from rotation caused by errors in the telescope pointing (Giles 1999; Beck et al. 2002). A Gaussian smoothing has been applied in the domains of time and latitude. The FWHMs in temporal and latitudinal smoothings are 1 yr and 7.°2, respectively.

Near the surface (Figure 1(a)), $\delta\tau_\infty$ at two minima has a typical sine-shape distribution in latitude, while $\delta\tau_\infty$ at the maximum deviates from the sine shape. In this study, this deviation from the $\delta\tau_\infty$ of minima is called the perturbation in $\delta\tau_\infty$. In Figure 1(b), the perturbations in $\delta\tau_\infty$ at the maximum are so large that the sign of $\delta\tau_\infty$ is reversed at low latitudes in both hemispheres. In the deeper layer (Figure 1(c)), the perturbations are smaller and shift to earlier time. In the even deeper layers (Figures 1(d) and (e)), the perturbations become small. The solar-cycle variations of $\delta\tau_\infty$ in Figure 1 are consistent with previous studies (Chou & Dai 2001; Beck et al. 2002; Chou & Ladenkov 2005; Kholikov & Hill 2014), although they have not gone as deep as this study. The perturbations in $\delta\tau_\infty$ correlate with the surface sunspot numbers (Chou & Ladenkov 2005). They have been interpreted as the result of an additional divergent flow being created at the active latitudes at the maximum and superposed on the undisturbed flow (Chou & Dai 2001; Beck et al. 2002).

3. EFFECTS OF SURFACE MAGNETIC FIELDS

Since the solar-cycle variations of subsurface meridional flow can be used to probe the subsurface magnetic fields, it is important to investigate whether the solar-cycle variations of $\delta\tau_\infty$ in Figure 1 are really the signals related to the subsurface meridional flow, not caused by the surface magnetic fields. To carry out the test, we remove the data points with field strength greater than a certain threshold: if one of the paired points used in CCF computation is inside a magnetic region with a strength greater than the threshold, the CCF of this pair is excluded in

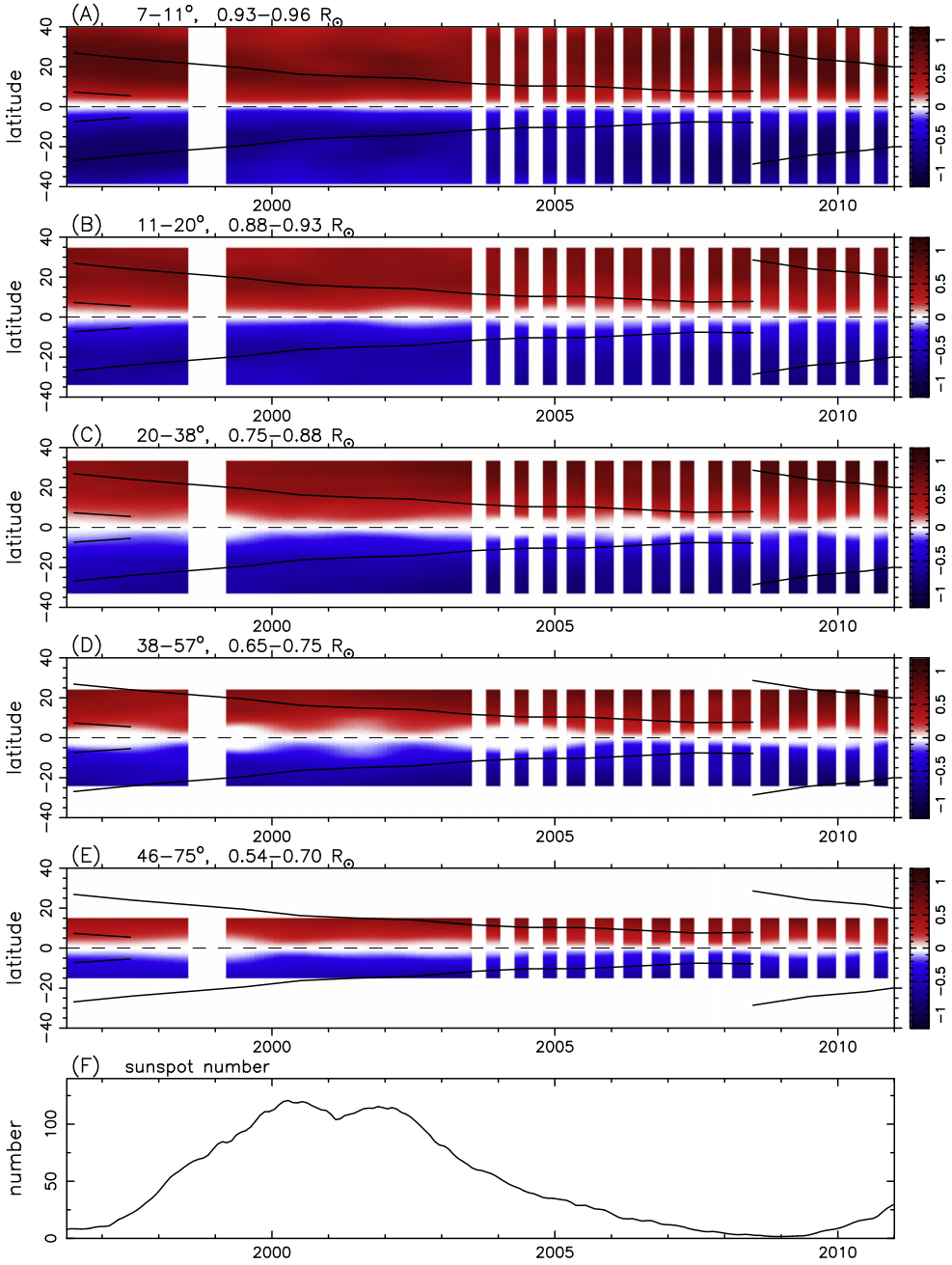

Figure 3. Travel time difference $\delta\tau_{50}$, with magnetic regions greater than 50 G removed, as a function of latitude and time for different travel distances.

averaging. It is noted that no spatial filter is applied to the data in this study to avoid the spreading of the influence of magnetic regions.

The magnetic data used here are the MDI 1024 × 1024 magnetograms taken at a rate of one image every 96 minutes. Each magnetogram is mapped into the longitude–latitude coordinates with a step size of 0.°12 in both directions. Then it is binned into the same size as the Dopplergram, with a step size of 0.°6. The daily-averaged magnetograms are used for removing surface magnetic area because each 24 hr Doppler time series is analyzed separately. The fraction of data points removed at each latitude for different thresholds is shown in Figure 2 for year 1997 (minimum) and year 2000 (maximum). The number of removed pairs in CCF computation is about twice the value in Figure 2.

The travel time difference computed with a threshold of 50 G, denoted as $\delta\tau_{50}$, is shown in Figure 3. It is clear that most of the perturbations disappear, especially those in the shallower layers (Figures 1(a)–(c)). This indicates that these perturbations are likely caused by the surface magnetic fields, and are unrelated to the meridional flow. This also suggests that the solar-cycle variations of meridional flow in these layers reported by the previous studies (Chou & Dai 2001; Beck et al. 2002; Chou & Ladenkov 2005; Kholikov & Hill 2014) are mainly caused by the surface magnetic effects. To see the large-scale structure of the surface magnetic effects as a function of latitude and time, we compute the difference between Figures 1 and 3, $\delta\tau_{\infty} - \delta\tau_{50}$, and the result is shown in Figure 4. Note that the range of color scale in Figure 4 is half of that in Figures 1 and 3. The effects of surface magnetic field are small at two minima, 1996 and

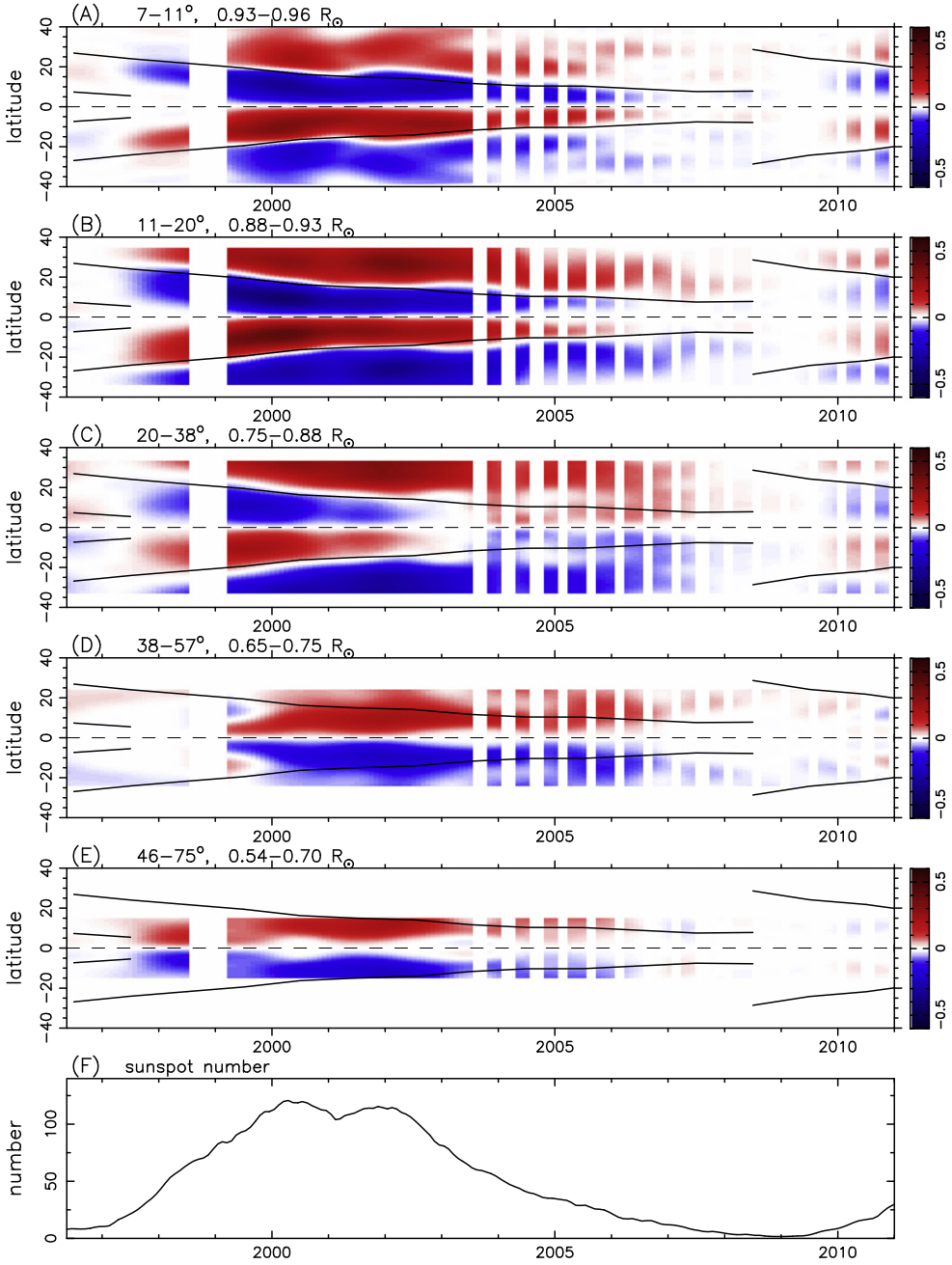

Figure 4. Difference $\delta\tau_\infty - \delta\tau_{50}$ as a function of latitude and time for different travel distances. Note that the range of the color scale is half of that in Figures 1 and 3.

2008–2009. However, they become noticeable in 1997 (beginning of cycle 23) and 2010 (beginning of cycle 24) when the surface activity is still weak. To see the detailed structure of the magnetic effects in latitude, $\delta\tau_\infty - \delta\tau_{50}$ in Figure 4 averaged over five different periods versus latitude is shown in Figure 5. Here only the northern hemisphere is shown because we keep only the antisymmetric part.

The surface effects are greatest at the maximum. Figures 4 (a) and (b) and 5(a) and (b) show that in the northern hemisphere $\delta\tau_\infty - \delta\tau_{50}$ is positive in the regions above the active latitudes and negative below the active latitudes. This phenomenon can be explained if there exists effective vertical downward flows inside magnetic regions near the surface.

If one of the paired points in the CCF computation is inside a magnetic region, the downflows at this point have opposite contributions to $\delta\tau_\infty$ around this point. In the northern hemisphere, the contribution of the downflows to $\delta\tau_\infty$ is positive at latitudes higher than this point and negative at latitudes lower than it, because $\delta\tau_\infty$ is assigned to the middle point between the pair. (The travel time difference is defined to be positive for northward motion and negative for southward motion.) Thus, the downflows at the active latitudes increase $\delta\tau_\infty$ in the regions above the active latitudes and decrease $\delta\tau_\infty$ in the regions below the active latitudes in the northern hemisphere, as shown in Figures 1(a) and (b). In Figure 1 (b), this effect is so large that $\delta\tau_\infty$ at the latitudes below the active latitudes reverses the sign.

The regions affected by the downflows move away from the active latitudes as the travel distance increases, and it eventually crosses the equator. If only part of it crosses the

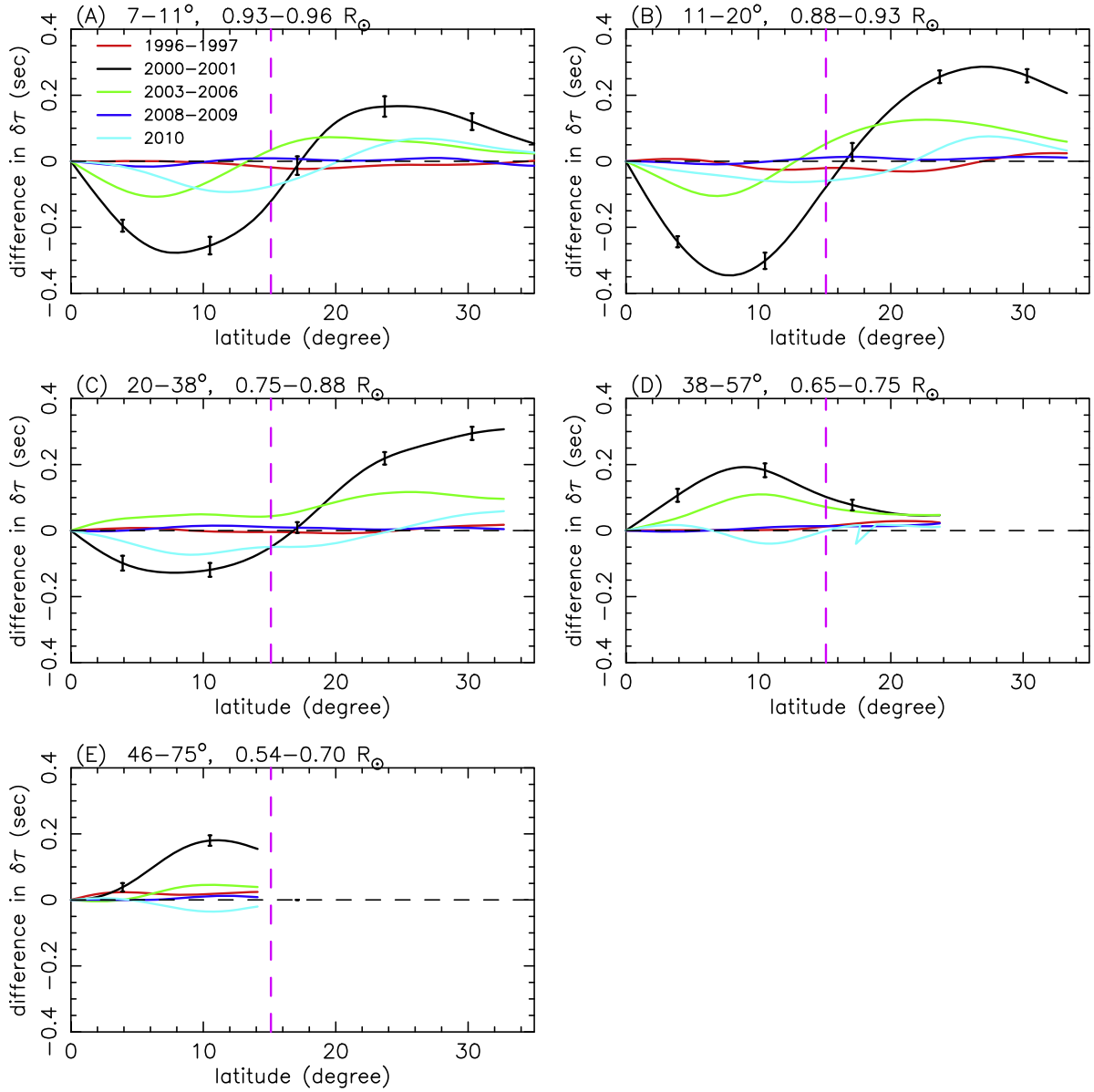

Figure 5. $\delta\tau_\infty - \delta\tau_{50}$ in Figure 4 averaged over five different periods vs. latitude. The vertical dashed line indicates the centroid of active latitudes at the maximum. Only the northern hemisphere is shown because only the antisymmetric part is kept.

equator, the surface effects at the low latitudes partially cancel with those coming from the opposite hemisphere. This indicates that the perturbations at low latitudes in Figure 1(c) are smaller than those in Figure 1(b) at the maximum, while more significant at the earlier time (year 1999) when the active latitudes are higher. This also accounts for the fact that $\delta\tau_\infty - \delta\tau_{50}$ in Figure 4(c) is weaker than that in Figure 4(b). If the travel distance increases further, such as in Figures 1(d) and (e), the affected regions completely cross the equator and enhance $\delta\tau_\infty$ in the opposite hemisphere. This effect shows as the phenomenon that the value of $\delta\tau_\infty - \delta\tau_{50}$ in Figures 4(d) and (e) at low latitudes changes the sign.

The effective vertical downflows in magnetic regions could also explain the smaller perturbations in Figure 1(a), in comparison with those in Figure 1(b). The ray with a smaller travel distance is less vertical near the surface, and it is less affected by the vertical downflows in magnetic regions. Thus, the perturbations in Figure 1(a) are smaller than those in Figure 1(b). Figure 4 shows that the effects of surface magnetic field are greatest for the travel distance 11°−20°, and become smaller as the travel distance is smaller or greater.

It should be emphasized that these effective downflows in magnetic regions appearing in the measured $\delta\tau_\infty$ are not related to the large-scale meridional flow. Figure 5 shows that the surface magnetic effect is small in the two minima (1996–1997 and 2008–2009). However, it is not negligible in 2010 when activity is still low. This indicates that the surface magnetic effects need to be considered if the travel time difference is used to infer meridional flow signals.

4. COMPARISON OF DIFFERENT MAGNETIC THRESHOLDS

It is of interest to know how the contribution of surface magnetic effect depends on the magnetic field strength. It is also important to know the appropriate threshold to remove most surface effects. It is clear that the smaller the threshold,

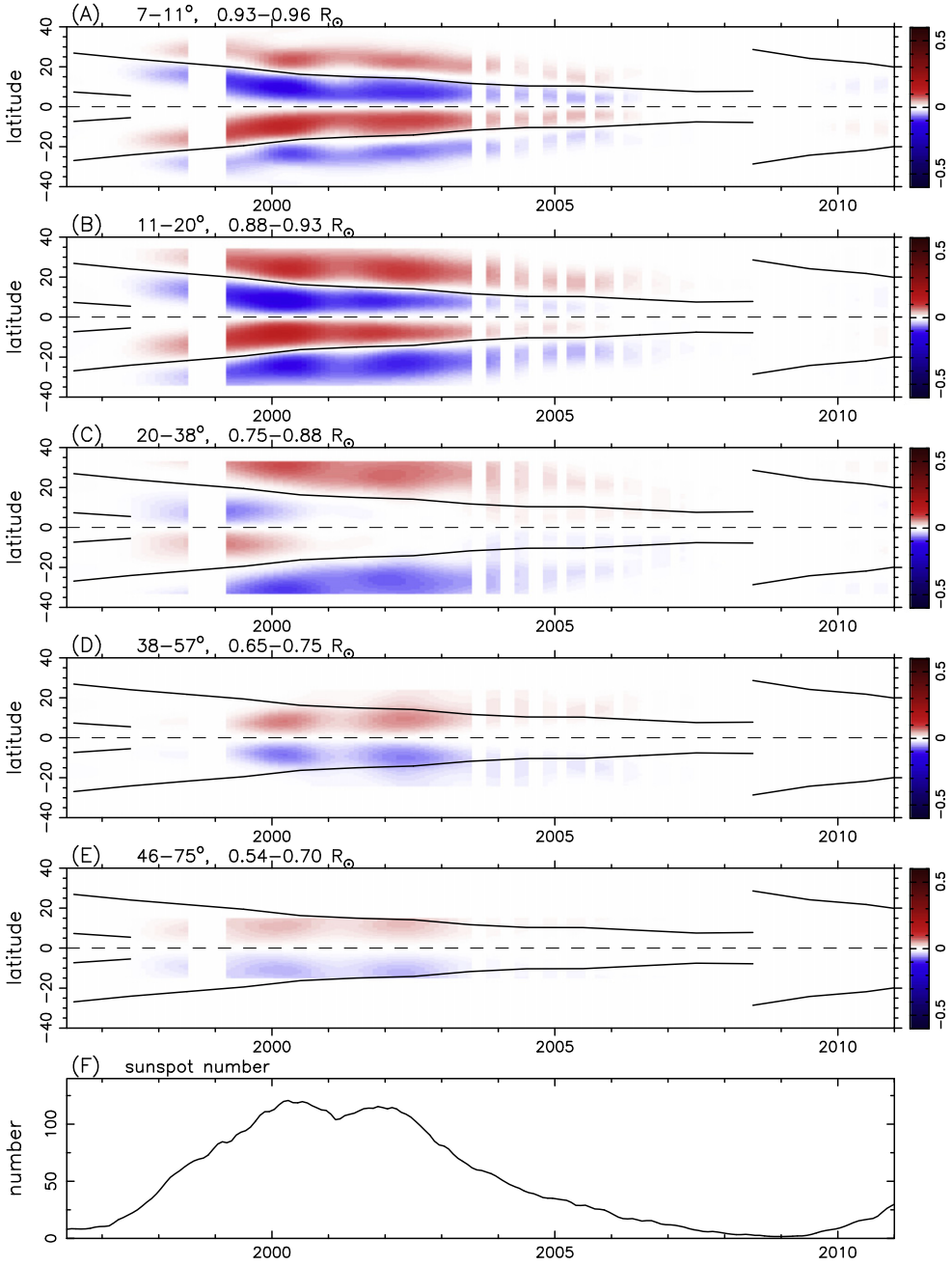

Figure 6. Difference $\delta\tau_\infty - \delta\tau_{600}$ as a function of latitude and time for different travel distances. The range of color scale is the same as Figure 4.

the less the contamination of the surface effects. However, the smaller the threshold, the smaller the number of data points left in the analysis and the lower the S/N. To find an appropriate threshold, besides a threshold of 50 G, discussed above, we also compute $\delta\tau$ for thresholds of 35, 75, 300, and 600 G. In the following discussion, the subscript of $\delta\tau_{\rm threshold}$ denotes the threshold of field strength. Figure 6 shows the difference $\delta\tau_\infty - \delta\tau_{600}$, which is significantly smaller than $\delta\tau_\infty - \delta\tau_{50}$ in Figure 4. It indicates that the magnetic area with strength less than 600 G has a significant contribution to the surface magnetic effects on travel time difference measurements, because the area of 50–600 G is much larger than that of above 600 G, shown in Figure 2.

For the comparison of the results using different thresholds, Figure 7 shows $\delta\tau_\infty$ and $\delta\tau_{\rm threshold}$ averaged over the maximum period (2000–2001) versus latitude for the different thresholds at five different depths (travel distances). Figure 8 shows the corresponding $\delta\tau_\infty - \delta\tau_{\rm threshold}$. Figures 7 and 8 show that the difference between $\delta\tau_{35}$ and $\delta\tau_{50}$ is less than 0.04 s. This suggests that using a threshold around 50 G can remove the surface magnetic effects within an accuracy of about 0.04 s for the highest activity (2000–2001).

For the successive thresholds, B and $B + \Delta B$, the difference between $\delta\tau_{B+\Delta B}$ and $\delta\tau_B$ divided by the difference in number of removed data points represents the contribution of each pixel in the range of $(B, B + \Delta B)$ to the surface magnetic effects. If the step ΔB is small enough, one can obtain the contribution to the surface magnetic effects as a function of field strength B. Such a study requires significant computational resources, and is not the goal of this study.

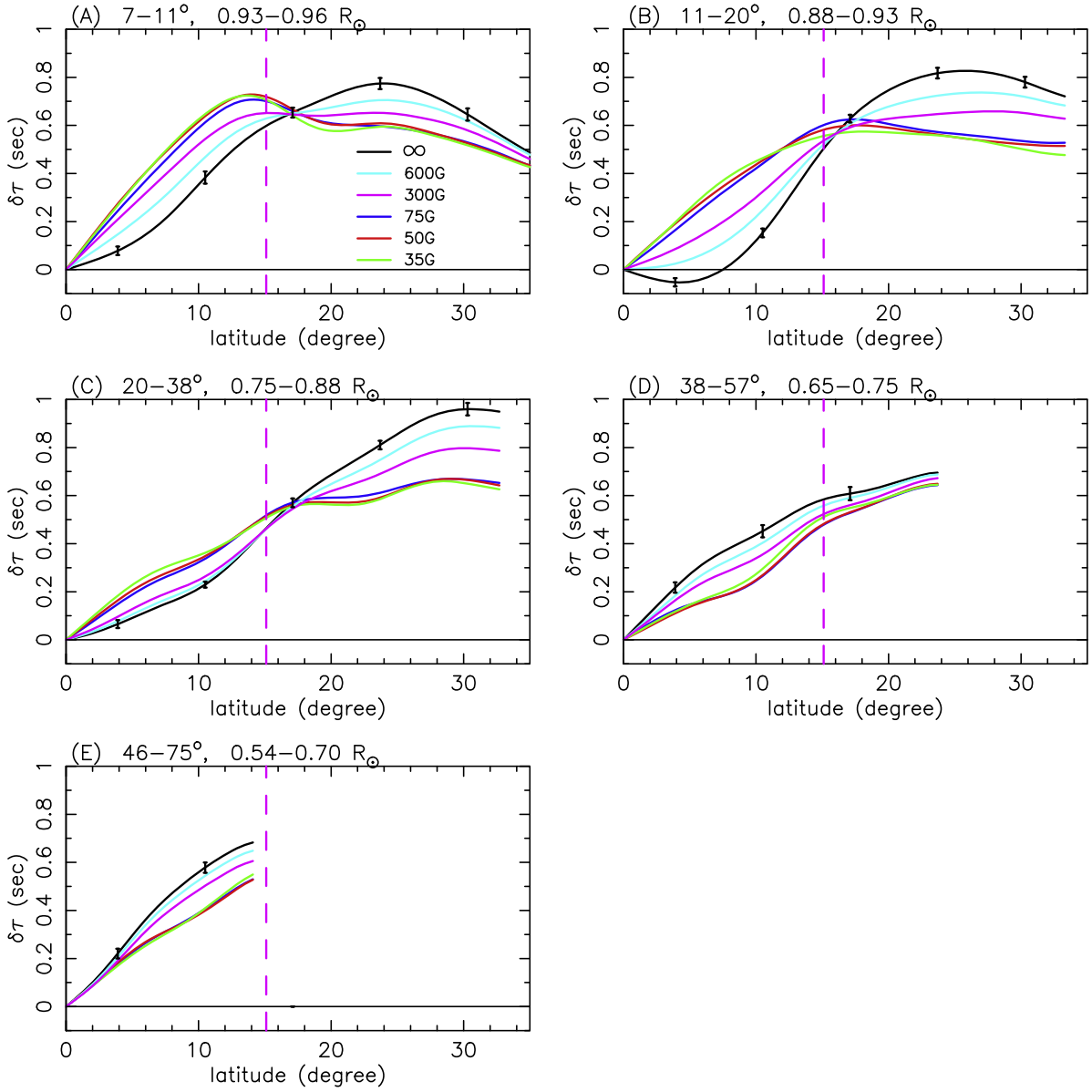

Figure 7. $\delta\tau_{\rm threshold}$ averaged over the maximum (2000–2001) vs. latitude for different thresholds at five different depths. Only the northern hemisphere is shown here because only the antisymmetric component is kept. The error is computed from the fluctuations in averaging. The errors of different curves are similar, and only the errors of one curve are shown here to avoid complication. The vertical dashed line indicates the centroid of active latitudes at the maximum.

5. SURFACE MAGNETIC EFFECTS ON MEAN TRAVEL TIME

With the measured northward and southward travel times, it is straightforward to obtain the mean travel time, which is the mean of opposite-direction travel times, denoted as $\bar{\tau}$. Here we also show the effects of surface magnetic regions on the mean travel time. The measured value of mean travel time suffers from unknown systematic effects and varies with time. Sometimes the variation is abrupt. To study the surface magnetic effects on the mean travel time, we compute the difference $\bar{\tau}_\infty - \bar{\tau}_{\rm threshold}$, where $\bar{\tau}_\infty$ is the mean travel time without removing magnetic area and $\bar{\tau}_{\rm threshold}$ the mean travel time using the threshold to remove magnetic area. The systematic effects other than the surface magnetic effect are removed in this difference.

The result of $\bar{\tau}_\infty - \bar{\tau}_{50}$ is shown in Figure 9. The fact that the value of $\bar{\tau}_\infty - \bar{\tau}_{50}$ is always negative indicates that the magnetic region reduces the mean travel time. This result is expected and similar to previous studies, although most previous studies have investigated only the upper convection zone. The shorter mean travel time is interpreted as the faster wave speed in magnetic regions (Duvall et al. 1996; Kosovichev 1996). This property has been used to probe the wave-speed perturbed regions in the upper convection zone (Kosovichev et al. 2000) (for more references, see the review by Gizon & Birch 2005). Similar to $\delta\tau_\infty - \delta\tau_{50}$ in Figure 4, the value of $\bar{\tau}_\infty - \bar{\tau}_{50}$ is also strongly correlated with the solar activity. The effects are visible even at the beginning of two solar cycles. The peak value of $\bar{\tau}_\infty - \bar{\tau}_{50}$ is not located at the active latitudes; instead, it is located below and above the active latitudes. This is more apparent for larger travel distances, such as Figures 9(c) and (d). It is because the mean travel time, like the travel time difference, is assigned to the middle point between the paired points used in CCF computation. Figure 9 shows that the value

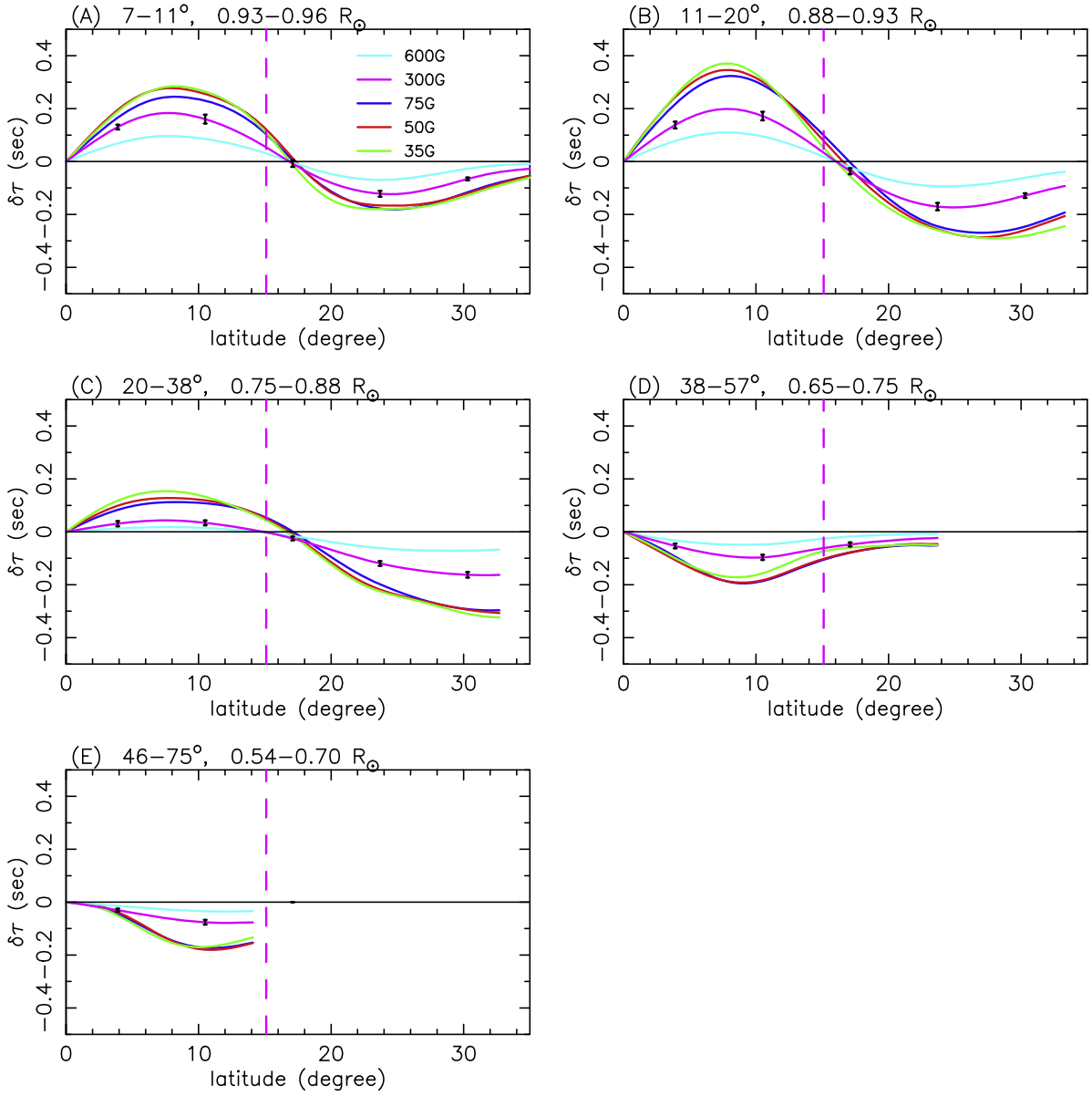

Figure 8. Same as Figure 7, but plotting $\delta\tau_\infty - \delta\tau_{\rm threshold}$. The error is computed from the fluctuations in averaging. The errors of different curves are similar, and only the errors of one curve are shown here to avoid complication. The vertical dashed line indicates the centroid of active latitudes at the maximum.

of $\bar{\tau}_\infty - \bar{\tau}_{50}$ is largest for 7°–11°, and decreases with travel distance.

For comparison, we also compute $\bar{\tau}_\infty - \bar{\tau}_{600}$, shown in Figure 10. The difference between $\bar{\tau}_\infty - \bar{\tau}_{600}$ and $\bar{\tau}_\infty - \bar{\tau}_{50}$ suggests that the magnetic area with strength less than 600 G has a significant contribution to the surface magnetic effects on mean travel time measurements, as the travel time difference.

6. SUMMARY AND DISCUSSION

We study the effects of surface magnetic fields on the measured travel time difference by comparing the results using data with and without removing surface magnetic regions. Two results are significantly different if the field strength threshold used to remove magnetic regions is small enough, for example, 50 G. The difference between two results represents the contribution from the surface magnetic regions. This difference can if be explained by effective downflows inside magnetic regions. However, it is unclear if this difference is caused by real downflows inside the magnetic regions (Duvall et al. 1996; Kosovichev 1996), or by the complication of the Doppler signal measured in the magnetic regions and appearing in the measured $\delta\tau$, including the shower-glass effect (Lindsey & Braun 2005), or by the combination of both.

The effects of the surface magnetic fields on the travel time difference discussed above are the near-surface phenomena. These local effects have been investigated by many authors (see the reviews by Gizon & Birch 2005 and Gizon et al. 2010). The previous studies use smaller travel distances to study local active regions in the upper convection zone, while here we use larger travel distances and smooth the results in space and time to study the large-scale flow in the entire convection zone. The local effective downflows in magnetic

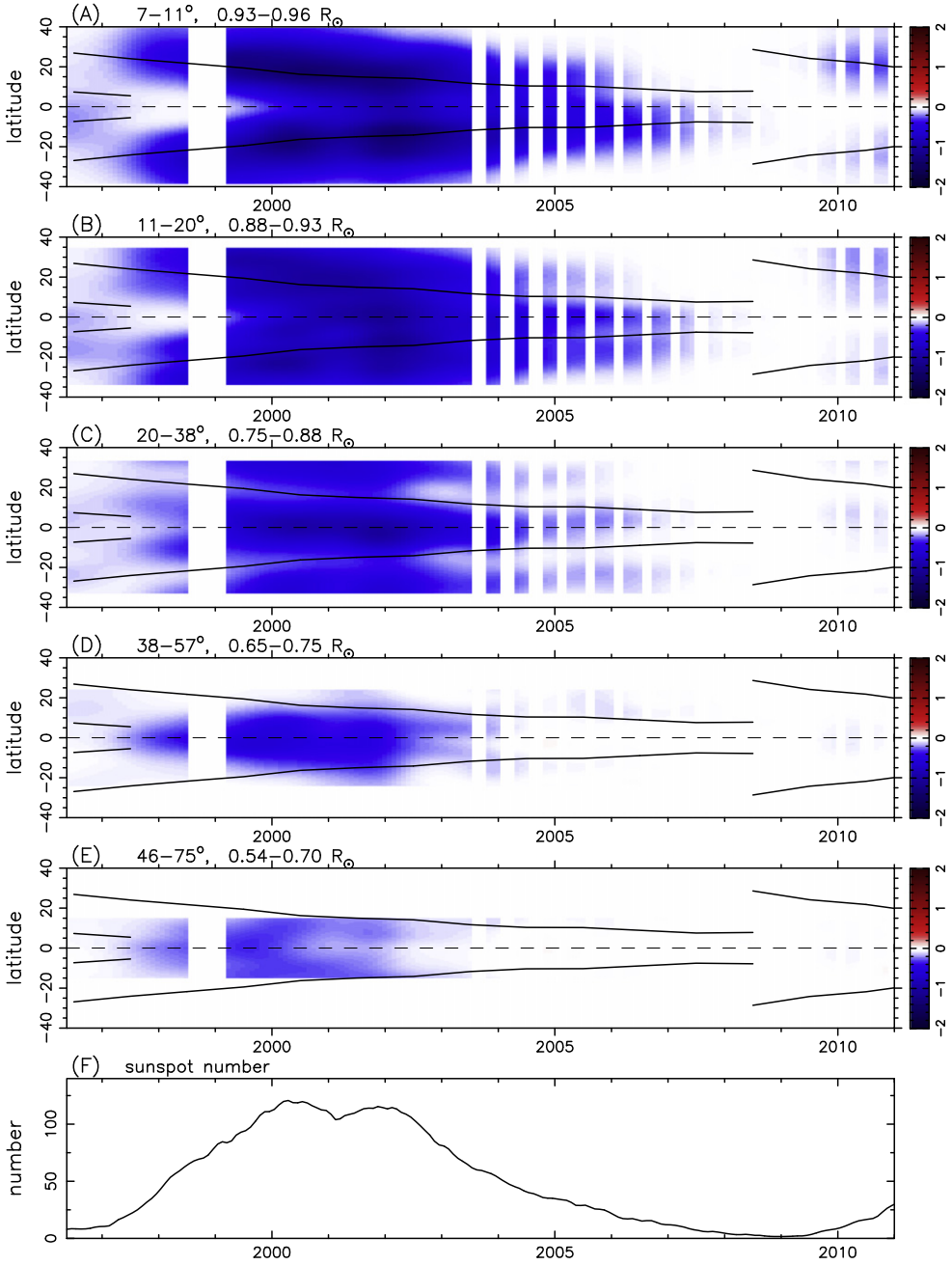

Figure 9. Difference $\bar{\tau}_{\infty} - \bar{\tau}_{50}$ as a function of latitude and time for different travel distances. The range of color scale is different from the previous figures.

regions are unrelated to the large-scale meridional flow. They need to be considered even when activity is low, if the measured travel time difference is used to infer meridional flow signals. The study with different field strength thresholds indicates that a threshold of about 50 G can remove most surface magnetic effects. If magnetic regions are included in travel time difference measurements, in principle, the local vertical flows and the large-scale flows are expected to be separated in the inversion of measured travel time difference if both components are included in the inversion.

The travel time difference without removing surface magnetic regions, $\delta\tau_{\infty}$, has a strong temporal variations associated with surface magnetic fields. In contrast, most solar-cycle variations in the travel time difference $\delta\tau_{50}$, removing magnetic regions with a threshold of 50 G, disappear. There still exists some residual solar-cycle variations in $\delta\tau_{50}$, especially near the base of the convection zone. To further investigate these residuals to see how they vary with the solar cycle and its inference on solar-cycle variations of meridional flow in the convection zone, one needs to deal with another systematic effect, the center-to-limb effect (Zhao et al. 2012). It is not the topic of this study.

SOHO is a project of international cooperation between ESA and NASA. The sunspot data in Figures 1, 3, 4, 6, 9, and 10 are from SIDC, Royal Observatory of Belgium. The authors are supported by the NSC of ROC under grant NSC-102-2112-M-007-022-MY3.

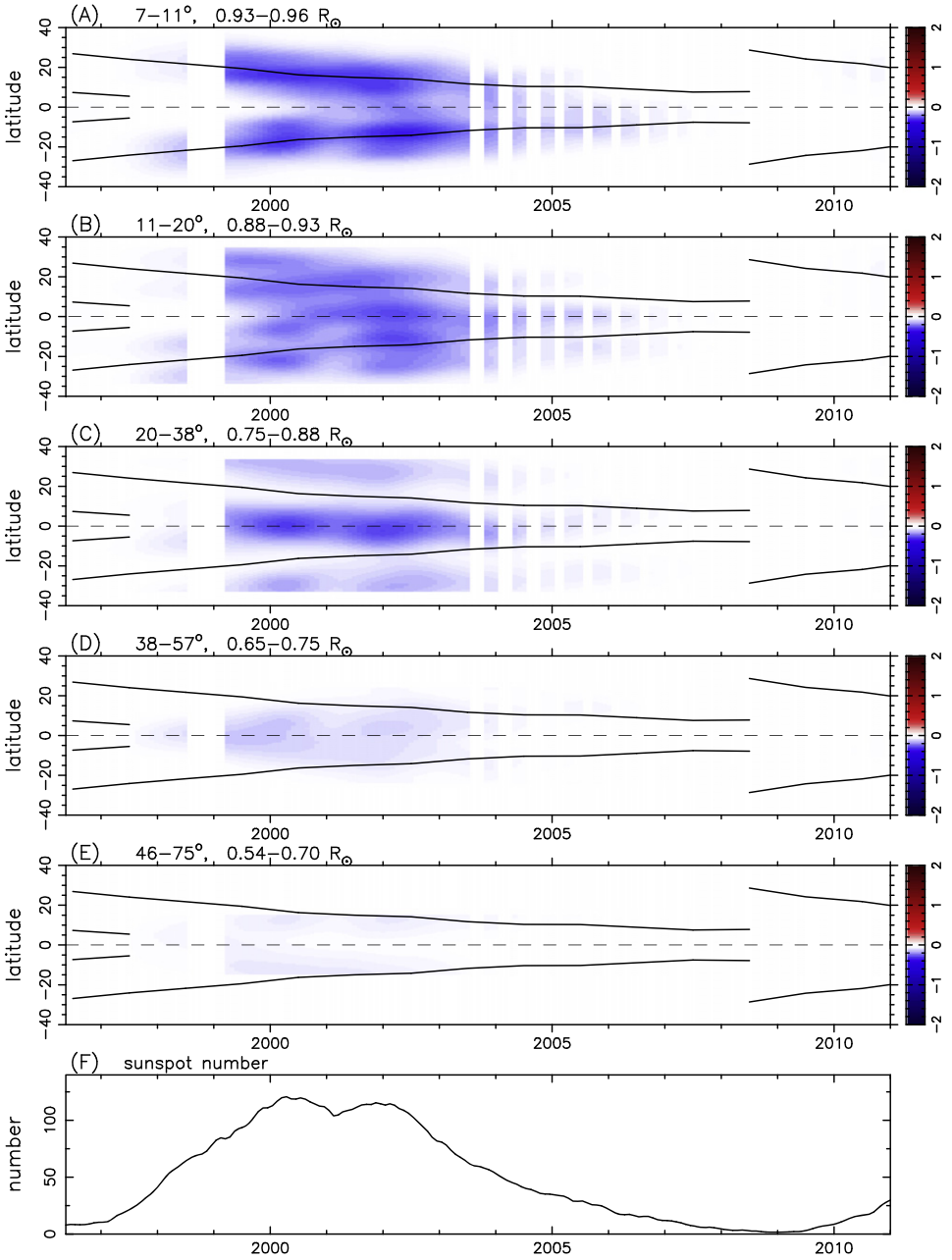

Figure 10. Difference $\bar{\tau}_{\infty} - \bar{\tau}_{600}$ as a function of latitude and time for different travel distances. The range of color scale is the same as Figure 9.

REFERENCES

Basu, S., Antia, H. M., & Tripathy, S. C. 1999, ApJ, 512, 458
Basu, S., & Antia, H. M. 2000, SoPh, 192, 469
Beck, J. G., Gizon, L., & Duvall, T. L., Jr. 2002, ApJL, 575, L47
Bracewell, R. N. 1986, in The Fourier Transform and Its Applications (2nd ed.; New York: McGraw-Hill)
Braun, D. C., & Fan, Y. 1998, ApJL, 508, L105
Chou, D.-Y., & Dai, D.-C. 2001, ApJL, 559, L175
Chou, D.-Y., & Ladenkov, O. 2005, ApJ, 630, 1206
Chou, D.-Y., Liang, Z.-C., Yang, M.-H., Zhao, H., & Sun, M.-T. 2009, ApJL, 696, L106
Chou, D.-Y., & Serebryanskiy, A. 2001, ApJL, 578, L157
Durney, B. R., & Roxburgh, I. W. 1971, SoPh, 16, 3
Duvall, T. L., Jr. 1979, SoPh, 63, 3
Duvall, T. L., Jr., D'Silva, S., Jefferies, S. M., Harvey, J. W., & Schou, J. 1996, Natur, 379, 235
Duvall, T. L., Jr., Jefferies, S. M., Harvey, J. W., & Pomerantz, M. A. 1993, Natur, 362, 430
Giles, P. M., Duvall, T. L., Jr., Scherrer, P. H., & Bogart, R. S. 1997, Natur,, 390, 52
Giles, P. M. 1999, PhD thesis, Stanford Univ.
Gizon, L. 2003, PhD thesis, Stanford Univ.
Gizon, L., & Birch, A. C. 2002, ApJ, 571, 966
Gizon, L., & Birch, A. C. 2005, LRSP, 2
Gizon, L., Birch, A. C., & Spruit, H. C. 2010, ARA&A, 48, 289
Gonzalez Hernandez, I., Kholikov, S., Hill, F., Howe, R., & Komm, R. 2008, SoPh, 252, 235
Hathaway, D. H., Gilman, P. A., Harvey, J. W., et al. 1996, Sci, 272, 1306
Hathaway, D. H., & Rightmire, L. 2010, Sci, 327, 1350
Howard, R., & Gilman, P. A. 1986, ApJ, 307, 389
Kholikov, S., & Hill, F. 2014, SoPh, 289, 1077
Kholikov, S., Serebryanskiy, A., & Jackiewicz, J. 2014, ApJ, 784, 145
Komm, R. W., Howard, R. F., & Harvey, J. W. 1993, SoPh, 147, 207
Kosovichev, A. G. 1996, ApJL, 461, L55
Kosovichev, A. G., Duvall, T. L., Jr., & Scherrer, P. H. 2000, SoPh, 192, 159
LaBonte, B. J., & Howard, R. F. 1982, SoPh, 80, 361
Lindsey, C., & Braun, D. C. 2005, ApJ, 620, 1107

Meunier, N. 1999, ApJ, 527, 967
Schad, A., Timmer, J., & Roth, M. 2011, ApJ, 734, 97
Schad, A., Timmer, J., & Roth, M. 2013, ApJL, 778, L38
Scherrer, P. H., Bogart, R. S., Bush, R. I., et al. 1995, SoPh, 162, 129
Snodgrass, H. B., & Dailey, S. B. 1996, SoPh, 163, 21
Svanda, M., Kosvichev, A. G., & Zhao, J. 2007, ApJL, 670, L69
Ulrich, R. K. 2010, ApJ, 725, 658
Zhao, J., & Kosvichev, A. G. 2004, ApJ, 603, 776
Zhao, J., Bogart, R. S., Kosvichev, A. G., Duvall, T. L., Jr., & Hartlep, T. 2013, ApJL, 774, L29
Zhao, J., Nagashima, K., Kosvichev, A. G., & Duvall, T. L., Jr. 2012, ApJL, 749, L5